



Fabrication of high mechanical properties papers coated with CMC-based nanocomposites containing nanominerals synthesized from paper waste

Faegheh Alsadat Mortazavi Moghadam · Hossein Resalati · Sousan Rasouli · Ghasem Asadpour

Received: 30 December 2020 / Accepted: 30 September 2021 / Published online: 12 October 2021
© The Author(s), under exclusive licence to Springer Nature B.V. 2021

Abstract In this work, nanokaolin (K) and nanometakaolin (MK) were synthesized from waste paper via planetary ball milling and characterized by means of X-ray diffraction (XRD), Fourier transform infrared vibrational spectroscopy (FTIR), and scanning electron microscopy (SEM). Suspensions of carboxymethyl cellulose (CMC) and the synthesized nanominerals at 1.5, 3, 6, and 9% led to nanocomposites 30, 60, 90, and 120 μm thick. Nanocomposites

coated papers were analyzed by means of XRD, FTIR, SEM, tensile index, strain rate, burst index, and air passage resistance. The highest tensile index, burst index, and air permeability resistance values of 80.78 $\frac{\text{N.m}}{\text{g}}$, 5.24 $\frac{\text{kPa.m}^2}{\text{g}}$, and 286.66 ml/min , respectively, were obtained for CMC-9%MK-120. These results indicated that paper coated with CMC nanometakaolin composite is suitable for packaging.

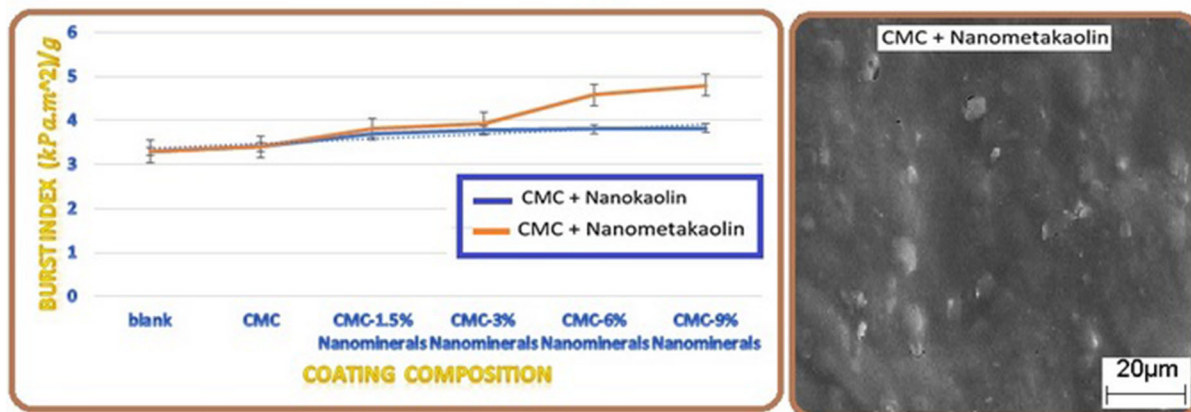
Supplementary Information The online version contains supplementary material available at <https://doi.org/10.1007/s10570-021-04241-7>.

F. A. Mortazavi Moghadam (✉) · H. Resalati · G. Asadpour
Department of Wood and Paper Science and Engineering,
Sari Agricultural Sciences and Natural Resources
University, Sari, Iran
e-mail: Mortazavi_faeghe@yahoo.com

S. Rasouli
Department of Nano Materials and Nano Coatings,
Institute for Color Science and Technology, Tehran, Iran

Graphic abstract

Fabrication of paper with high mechanical properties by using synthesized nanominerals from paper waste and CMC



Keywords Nanokaolin · Nanometakaolin · Coating · CarboxyMethyl cellulose (CMC) · Mechanical and microstructural properties

Introduction

Coating processes as well as nanomaterials can be used to improve different properties of papers such as mechanical properties, permeability, appearance, etc. (Singhal et al. 2015). In recent years, several biopolymers have been used as coatings for paperboards and papers. These biopolymers must be capable of forming films and can be classified into several main groups: polysaccharides (starch, cellulose and its derivatives, chitosan, and alginate, etc.), proteins (casein, whey protein, soy, collagen, and gluten, etc.), lipids (honey wax, carnauba wax, free fatty acid, etc.), and polyesters (polyhydroxyalkanoates (PHA), polylactic acid (PLA), etc.). Among these, cellulose derivatives have found wide applications for paper coating. (Manzel et al. 2014). However, some disadvantages of biopolymers are insufficient adhesion, layered structure, and layered fragility, which lead to a non-uniform coating on the paper. However, cellulose derivatives such as carboxymethyl cellulose (CMC) can provide the suitable adhesion and absorption properties as the paper because their coordination and

structure are similar to those of the base paper, thus creating a uniform coating.

On the other hand, the properties of biopolymers can be improved by the addition of micrometer or nanometer size materials or fillers to make composites (Rastogi et al. 2015; Rong et al. 2006). Biological and inorganic resources such as nanocellulose and nanoclay (nanokaolin) are examples of such nanomaterials. Paper wastes, such as paper sludge, contain significant amounts of kaolin (Gurram et al. 2015; Prasetyo et al. 2013), which can be converted to nanokaolin and nanometakaolin for paper coating.

Kaolin ($\text{Al}_2\text{Si}_2\text{O}_5(\text{OH})_4$) is chemically stable under various chemical conditions and can be used in a variety of papermaking methods (Hubbe et al. 2016; Murray et al. 1961). Kaolin is used as a filler and coating in the paper industry and can enhance some paper properties, such as printability. Kaolin modification requires expensive and time-consuming treatments such as sedimentation, bleaching, etc. (Morsy et al. 2014).

Metakaolin has a layered structure with higher reactivity than kaolin (Kenne Diffo et al. 2015; Huseien et al. 2018).

Current work, for the first time, reports the extraction of kaolin from waste paper, synthesis of metakaolin, and production of nanomaterials via planetary ball mill for enhancing the mechanical properties of coated papers.

In this work, metakaolin has been converted to nanometakaolin to increase its functional properties. In other words, nanomaterials can be dispersed in suspension more easily than micro-scale materials because they have higher specific surface area. Numerous reports have been published on paper coating, but so far none of them used nanometakaolin in their coating formulations. Also, no research has been done on nanometakaolin/carboxymethyl cellulose (CMC) nanocomposites for paper coating. As a result, in this research, nanokaolin and nanometakaolin were used in coating formulations instead of kaolin and metakaolin, and the properties of the coated papers were investigated. For this purpose, kaolin was initially extracted from paper waste, and then metakaolin was synthesized from the extracted kaolin. X-ray diffraction (XRD), Fourier transform infrared spectroscopy (FTIR), and scanning electron microscopy (SEM) techniques were used to investigate the structure, microstructure, functional groups, and morphology of nanometakaolin and nanokaolin.

The synthesized nanoparticles were used in CMC-based nanocomposites for the paper coating. Then tensile strength and burst strength of the coated paper were evaluated. XRD and SEM were also utilized to investigate the chemical composition, surface structure, and morphology of the coatings.

Materials and methods

In this study, papers (80 g/m²) made by COPIMAX Co, Thailand, were used to extract the kaolin as raw materials. Hydrochloric acid (99% purity) and carboxymethyl cellulose (99% purity) were purchased from Merck Co. and Kimia Tehran Acid Co., respectively.

Extraction and analysis of kaolin

The paper samples were shredded and burned. After passing through a 120-mesh sieve, the residual ash samples were placed alumina ceramic crucibles and combusted in an electric furnace at 550 °C for 1 h in air. The paper ash was washed with hydrochloric acid to remove the acid-soluble minerals (such as calcium carbonate), rinsed with distilled water, and dried at 120 °C for 24 h. The extracted kaolin was analyzed by XRD and FTIR methods. Finally, the synthesized

kaolin was heat-treated at 850 °C temperatures for 6 h to produce metakaolin, which was then analyzed by XRD and FTIR.

Production of nanoparticles

Planetary ball mill (Retsch, PM 100, Germany; with a 200 cc zirconia cup and PLC for adjusting the rotational speed and milling time) was used to prepare nanokaolin and nanometakaolin. The particles were ball milled at ball-to-powder-ratio (BPR) of 20 to 1 and mill rotary speed of 400 rpm for 90 min under the argon gas atmosphere to prevent moisture absorption. The nanoparticles were also analyzed by SEM after milling.

Handmade base-paper

FRANK-PTI handmade paper machine (P41521.159, Austria) was used to make handmade papers from the bleached softwood Kraft pulp (supplied by ILIM Co., Russia) as the base paper for coating experiments, according to T 205 SP-02 standard. The handmade papers were also conditioned according to T 402 sp-98 standard.

Preparation of coating suspension

Water-based solution of 1% (w:v) carboxymethyl cellulose (CMC) was prepared. Then, the synthesized nanomaterials were added to the suspension at 1.5, 3, 6, and 9 wt%) and homogenized at 10,000 rpm for 3 min by Ultra-Turrax—IKA T25 Digital Homogenizer (IKA Co, Germany). Coating of the handmade base paper was performed by an automatic coating machine (Dongguan Lonroy Equipment, China) with four different coating thicknesses levels (30, 60, 90, and 120 μm). The coated papers were dried with UV-IR Laboratory Dryer BE 20 (Systec Co, Germany). After drying, all samples were examined by coating thickness gauge PT-200-S3 advanced (PCE, Co, USA) to obtain uniform coating thickness.

Coating analysis

Tensile strength was measured by GOTECH AI-300 machine, according to TAPPI T 404 om-92 standard. Burst strength was determined by burst strength tester DRK 109, according to TAPPI T 403 om-97 standard.

Air permeability resistance was measured by Gurley method according to TAPPI T 460 om-96 standard.

The number of tests is three times the standard for each treatment. For example, in the tensile test, the standard value is ten samples done three times in this research. In other words, for each type of treatment, the tensile tests were performed for thirty samples; the average value was reported for each type of treatment. Statistical analysis of data was performed using one-way analysis of variance (ANOVA) and a completely randomized design. The mean values were compared by Duncan's multiple range test (DMRT) at the level of 5% probability; significant difference was related to $\alpha < 0.05$. XRD, FTIR, and SEM analyses were also performed to examine the coated papers' surface and microstructure properties.

X-ray diffraction (XRD) patterns were reformed on Philips PW3710 XRD device, working with Cu-K α ($\lambda = 0.154$ nm, 40 kV, and 30 mA). The diffraction patterns were collected at 25 °C in the 2θ range of 10 to 90° with a step size of 0.02°. FTIR spectra were recorded on a Nicolet FTIR Nexus 870 instrument (KBr discs) in the range of 400–4000 cm $^{-1}$ with a resolution of 2 cm $^{-1}$. The microstructure and morphology of the samples were examined by scanning electron microscope (SEM, TESCAN VEGA II XMU) after coating with gold. The flow chart in Fig. S1 (Supporting Information) shows the sample preparation and characterization steps. Table 1 describes the prepared samples and their codes.

Results and discussion

Characterization of recycled kaolin and synthesized of metakaolin

Removal of cellulose and other impurities from paper waste is necessary for kaolin extraction. Thus, the paper ash was washed with hydrochloric acid for removing contaminants such as calcium carbonate (CaCO $_3$), according to the following equation:

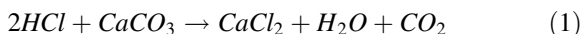


Figure 1 shows FTIR spectra and XRD patterns of both the extracted kaolin and the synthesized metakaolin.

The XRD pattern of kaolin is shown in Fig. 1a. The kaolinite peaks are located at 2θ , 12.36°, 20.21°,

25.49°, and 38.46° consistent with JCPDS 01–089-6538. Therefore, the sample is mainly composed of the kaolinite phase. Also, quartz (JCPDS 00-002-0471), small amount of illite (JCPDS,01–070-3754), and anatase (01-071-1167) phases existed as minor impurities. The crystal structure of kaolin is triclinic with $a = 5.15$ Å, $b = 8.94$ Å, and $c = 7.39$ Å. These findings are consistent with the previously reported studies (Walkley et al. 2019; Rakhimova et al. 2019; Asadi et al. 2012). A broad peak can be seen in the diffraction pattern of metakaolin between $2\theta = 20$ –30°. The kaolinite peak at $2\theta = 12.36^\circ$ was removed after the calcination process, resulted in the formation of metakaolin. It indicates that the kaolin network in [001] direction has been destroyed (Li et al. 2018; Asadi et al. 2013). Metakaolin has an amorphous structure, and the highest diffraction peaks correspond to the presence of quartz (SiO $_2$), which is very common (Fig. 1a). The only crystalline phases in metakaolin are quartz and small amounts of illite and anatase phases. Also, the absence of calcium oxide (CaO) peaks in the sample indicates that the sample has been thoroughly cleaned after washing with hydrochloric acid. Figure 1b shows the comparison between the FTIR spectra of recycled kaolin and the synthesized metakaolin. The peak at 1031 cm $^{-1}$ corresponds to asymmetric stretching vibration of Si–O–Si or Si–O–Al bonds (Asadi et al. 2013). The peak has been shifted to higher wavenumber of 1089 cm $^{-1}$, after heat treatment and conversion to metakaolin, indicating that the bonds have been broken and metakaolin has been formed. The kaolinite characteristic peak at 537 cm $^{-1}$ is related to Si–O–Al bonds. This peak disappeared after metakaolin formation. The stretching vibration bonds of Al–OH with 6-point coordination at 911 cm $^{-1}$ in the kaolin spectrum disappeared. After metakaolin formation because the coordination number of hexagonal aluminum changes form 6 to 4 or 5. (Lorentz et al. 2018). Also, the peaks at 3619 and 3696 cm $^{-1}$ are related to kaolinite which also disappeared after metakaolin formation.

Figure 2a1 and b1 show crystalline particles before milling, which changed to fine rounded particles after milling (Fig. 2a2, a3 and b2, b3); the average particle size decreased to less than 100 nm after milling process.

Table 1 coating description and sample codes

| Coating | Wet coating thickness (μm) | Nanokaolin (Wt%) | Nanometakaolin (Wt%) | Sample code | |
|---------------------------|---|------------------|----------------------|---------------|----------------|
| CMC without nanomaterials | 30 | | | CMC-30 | |
| | 60 | | | CMC-60 | |
| | 90 | | | CMC-90 | |
| | 120 | | | CMC-120 | |
| | 30 | 1.5% | | CMC-1.5%K-30 | |
| | 60 | 1.5% | | CMC-1.5%K-60 | |
| | 90 | 1.5% | | CMC-1.5%K-90 | |
| | 120 | 1.5% | | CMC-1.5%K-120 | |
| CMC with nanokaolin | 30 | 3% | | CMC-3%K-30 | |
| | 60 | 3% | | CMC-3%K-60 | |
| | 90 | 3% | | CMC-3%K-90 | |
| | 120 | 3% | | CMC-3%K-120 | |
| | 30 | 6% | | CMC-6%K-30 | |
| | 60 | 6% | | CMC-6%K-60 | |
| | 90 | 6% | | CMC-6%K-90 | |
| | 120 | 6% | | CMC-6%K-120 | |
| | 30 | 9% | | CMC-9%K-30 | |
| | 60 | 9% | | CMC-9%K-60 | |
| | 90 | 9% | | CMC-9%K-90 | |
| | 120 | 9% | | CMC-9%K-120 | |
| | CMC with nanometakaolin | 30 | | 1.5% | CMC-1.5%MK-30 |
| | | 60 | | 1.5% | CMC-1.5% MK-60 |
| | | 90 | | 1.5% | CMC-1.5%MK-90 |
| | | 120 | | 1.5% | CMC-1.5%MK-120 |
| 30 | | | 3% | CMC-3%MK-30 | |
| 60 | | | 3% | CMC-3%MK-60 | |
| 90 | | | 3% | CMC-3%MK-90 | |
| 120 | | | 3% | CMC-3%MK-120 | |
| 30 | | | 6% | CMC-6%MK-30 | |
| 60 | | | 6% | CMC-6%MK-60 | |
| 90 | | | 6% | CMC-6%MK-90 | |
| 120 | | | 6% | CMC-6%MK-120 | |
| 30 | | | 9% | CMC-9%MK-30 | |
| 60 | | | 9% | CMC-9%MK-60 | |
| 90 | | | 9% | CMC-9%MK-90 | |
| 120 | | | 9% | CMC-9%MK-120 | |

Characterization of papers coated with CMC nanocomposites

Figure 3 depicts the effect of nanoparticles loading on the tensile strength. Figure 3a and b show Three-dimensional (3D) representation of tensile strength

variations versus coating composition and the levels changes of the tensile index for each treatment, respectively. It can be seen that nanomaterials have positive effect and increased the tensile strength of the paper in the samples containing nanometakaolin (MK samples). There is an increase in the tensile strength

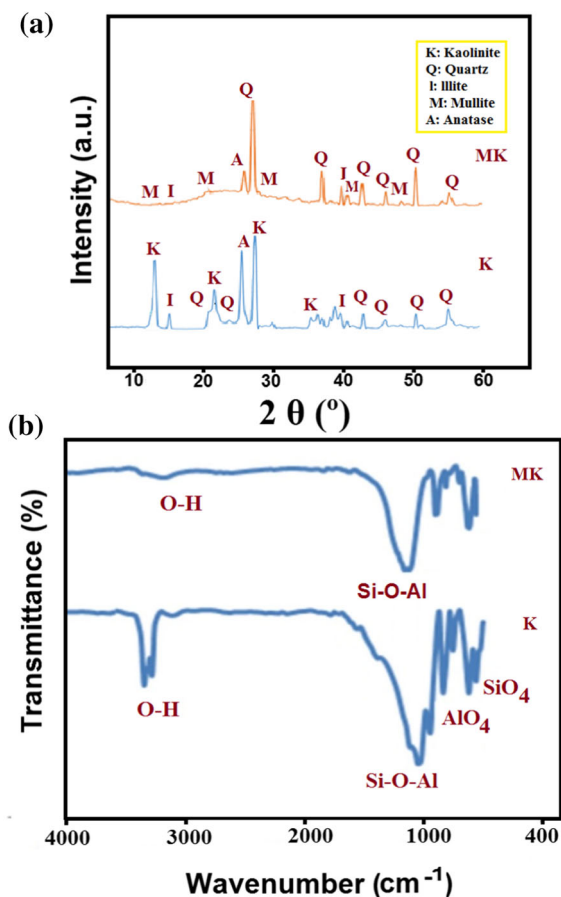


Fig. 1 (a) XRD patterns and (b) FTIR spectra of the recycled kaolin (K) and the synthesized metakaolin (MK)

that can be attributed to the better interaction between the nanometakaolin and the biopolymer matrix in comparison with nanokaolin. Also, Fig. 3c and d depict the effect of nanoparticles loading on strain and the levels changes of the strain for each treatment, respectively. Figure 3c and d show that both nanocomposite samples have an increasing trend compared to the control sample (Fig. 3c and d). In addition, the lowest tensile index and strain value are related to the control sample; samples with CMC coating showed less tensile strength and strain than CMC-K and CMC-MK nanocomposite coatings. The highest tensile strength and strain were obtained for CMC-9%MK-120 example, indicating better distribution of nanometakaolin in the CMC matrix than nanokaolin, thus creating more compatible coating with the base paper. Tensile strength of sample CMC-9%MK-120 was the highest and showed a significant

difference ($\alpha < 0.05$) with sample CMC-9% K-120. However, a significant difference ($\alpha < 0.05$) was found for tensile strength values across samples CMC-K and CMC-MK. As a result, nanometakaolin showed better performance than nanokaolin in improving the properties of polymer nanocomposite coatings. For tensile strength and strain, increasing the nanominerals concentration in formulation coating increased significantly the tensile index and strain ($\alpha < 0.05$) for samples CMC-K, CMC-MK. In general, nanomaterials can improve the tensile strength of coatings. This increase in tensile strength and strain rate can be attributed to the strength, orientation, high aspect ratio, and uniform distribution of nanoparticles in the polymer matrix. The coated paper should have good tensile strength and flexibility to withstand the stresses and strains applied in different applications. Therefore, it has been concluded that although the proper distribution of nanometakaolin is essential in improving the mechanical properties of nanocomposites, the interaction between the filler and the matrix is also important.

The burst strength of the samples is depicted in Fig. 4. Figure 4a and b show Three-dimensional (3D) representation of burst index variations versus coating composition and thickness ($\alpha < 0.05$) of biopolymer nanocomposite coating on the paper burst index and levels changes of burst index for each treatment, respectively.

Burst strength is the hydraulic pressure required to tear paper that enters a 30.5 mm aperture, and it is sometimes said that the burst strength is closely related to the tensile strength. This statement is based on stresses distribution during the experiment. As shown in Fig. 4, all the coatings have positive effect on the burst strength. Burst strength of sample CMC-9%MK-120 was the highest and showed a significant difference ($\alpha < 0.05$) with sample CMC-9% K-120. However, a significant difference ($\alpha < 0.05$) was found for burst strength values across samples CMC-K and CMC-MK. The coatings with nanometakaolin and nanokaolin were more effective than those without these nanominerals. Figure 4b shows that CMC-MK coatings increased significantly the paper burst strength mainly due to the high specific surface area and the existence of functional groups in metakaolin nanoparticles, leading to better bonding and more uniform coverage of the base paper in comparison with the two other samples (i.e. CMC and CMC-K

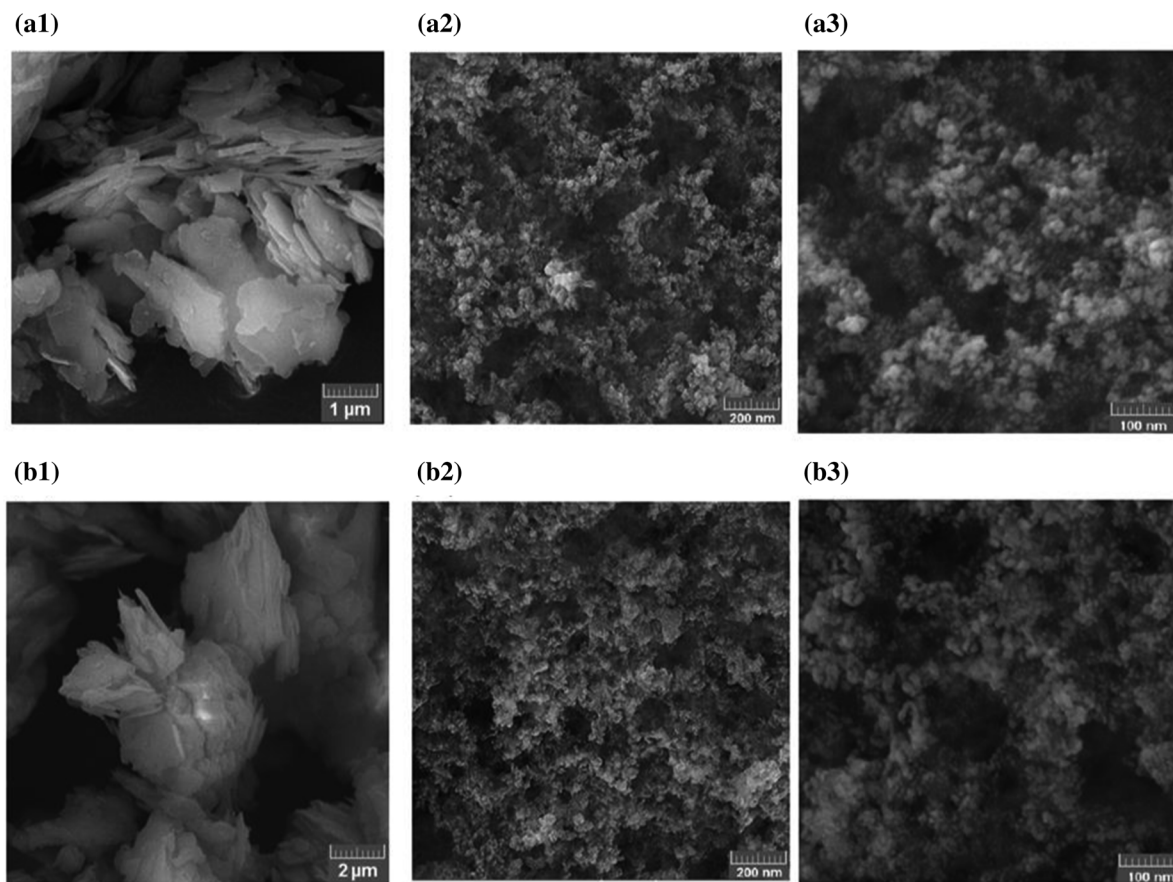


Fig. 2 SEM images of (a) synthesized metakaolin, and (b) recycled kaolin; (a1) and (b1) before milling and (a2, a3) and (b2, b3) after milling at different magnifications

samples). It can be seen that by increasing the concentration of metakaolin nanoparticles and thickness of coating, burst strength increases considerably.

Figure 5a and b show Three-dimensional (3D) representation of air passage resistance and levels of air passage resistance changes in various coating formulations and thickness ($\alpha < 0.05$), respectively. It is obvious that the air passage of the coated paper is much less than the blank sample (uncoated paper). Also, the air permeability of papers decreases with increasing the coating thickness, and there is a significant difference between all samples ($\alpha < 0.05$). The highest value is related to CMC-9%MK-120 ($\alpha < 0.05$). Also, it is observed that the effect of paper coating containing nanometakaolin is higher than nanokaolin. In general, the results indicate that the permeability properties change with coated layer thickness and the pores have blocked with

increasing the percentage of nanomaterials and coating thickness (less porosity).

Figure 6 shows XRD patterns and FTIR spectra of CMC-K, CMC-MK, and CMC. The XRD pattern of CMC-MK coating in Fig. 6a shows that this sample is amorphous. The broad peak indicates the presence of CMC and metakaolin. There is an amorphous peak overlap of CMC and metakaolin in the range of 20–30°. The XRD pattern of CMC-K coating is also shown in Fig. 6a. The peaks of kaolin phase can be seen at 12.36, 20.21°, and 25.49°. In contrast to CMC-MK sample, CMC-K sample is crystalline, which confirms the higher reactivity of CMC-MK compared to CMC-K sample. Figure 6b compares FTIR spectra of CMC, CMC-K, and CMC-MK samples. In the FTIR spectrum of the CMC sample, the absorption peaks at 3424, 2900, 1437, and 1060 cm^{-1} correspond to the presence of O–H, CH, C = O, and CH–O–CH groups.

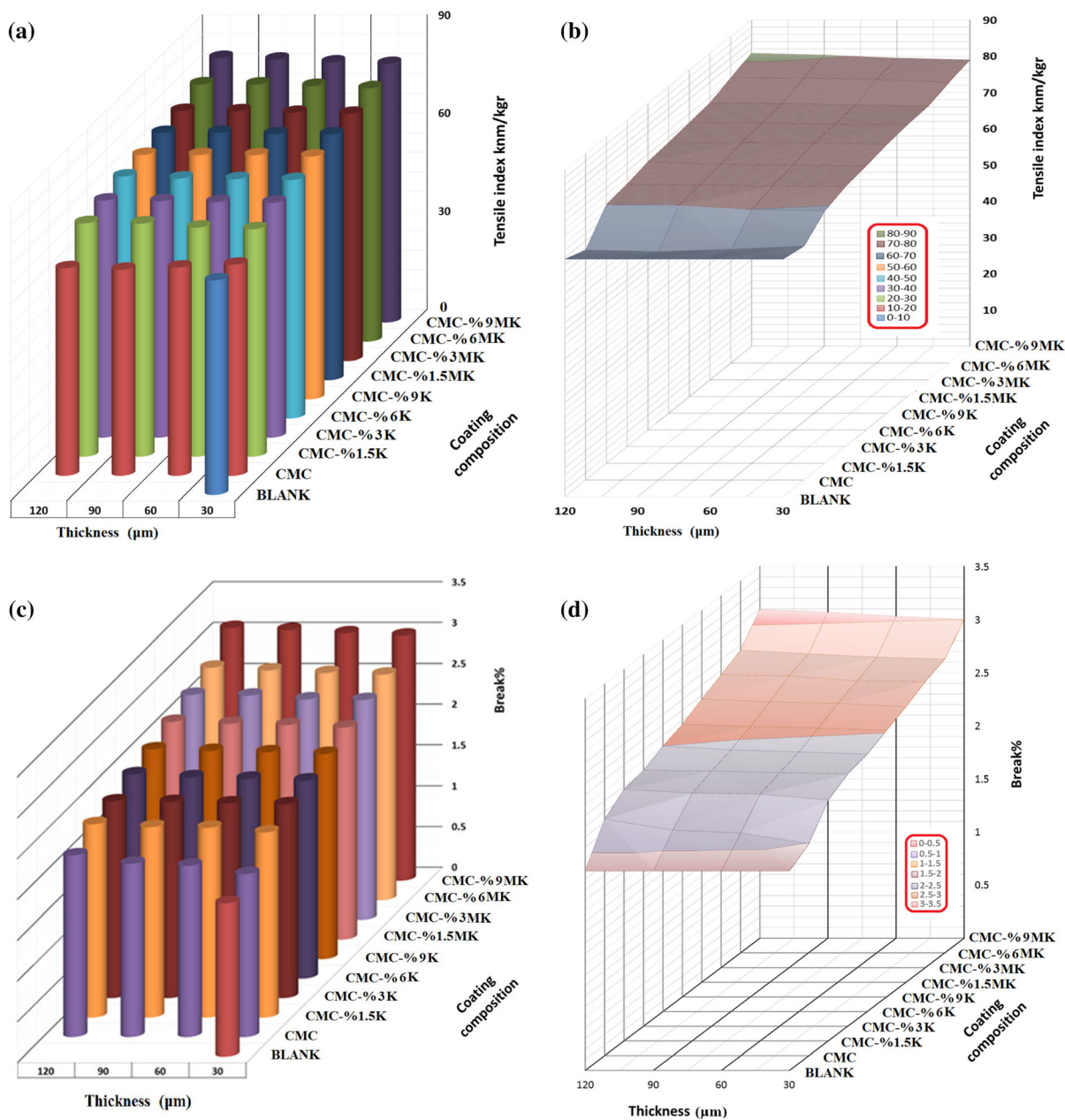


Fig. 3 Three-dimensional (3D) representation of tensile strength variations versus coating composition and thickness of the samples ($\alpha < 0.05$): (a) tensile index, (b) levels changes of tensile index, (c) strain change diagram, and (d) the levels of strain

The broad absorption band at around 3430 cm^{-1} is related to the of O–H group of cellulose hydroxyls. The peak at around 2900 cm^{-1} is attributed to the C–H of CH_2 and CH_3 groups. The absorption peak at 1600 cm^{-1} confirms the presence of carboxylic COO groups while the bands at 1300 cm^{-1} and 1400 cm^{-1} are related to the vibration of methyl group and the

bending vibration of hydroxyl group, respectively. The absorption band at around 1050 cm^{-1} can be assigned to the of CH–O–CH group. Peaks at 1737 cm^{-1} and 1228 cm^{-1} confirm the presence of C = O and C–O bonds of carboxylic acid, respectively. The FTIR spectrum of CMC-K nanocomposite in Fig. 6b shows two absorption peaks. One is related to CMC,

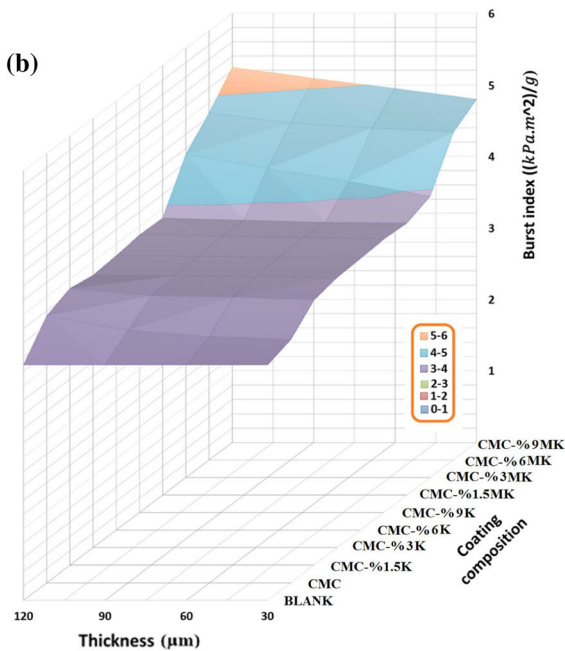
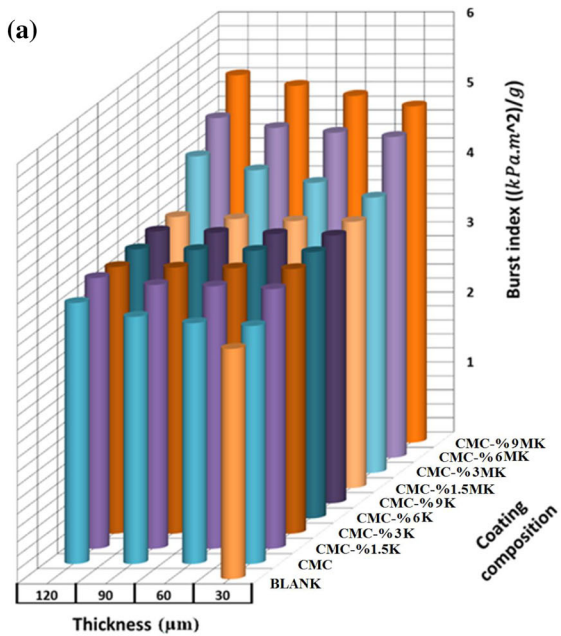


Fig. 4 Three-dimensional (3D) representation of burst index variations versus coating composition and thickness ($\alpha < 0.05$); (a) burst index, (b) levels changes of burst index for each treatment

and the other is related to kaolin. The broad absorption band at around 3430 cm^{-1} is related to the O–H of OH functional group. The peak at around 2900 cm^{-1} is

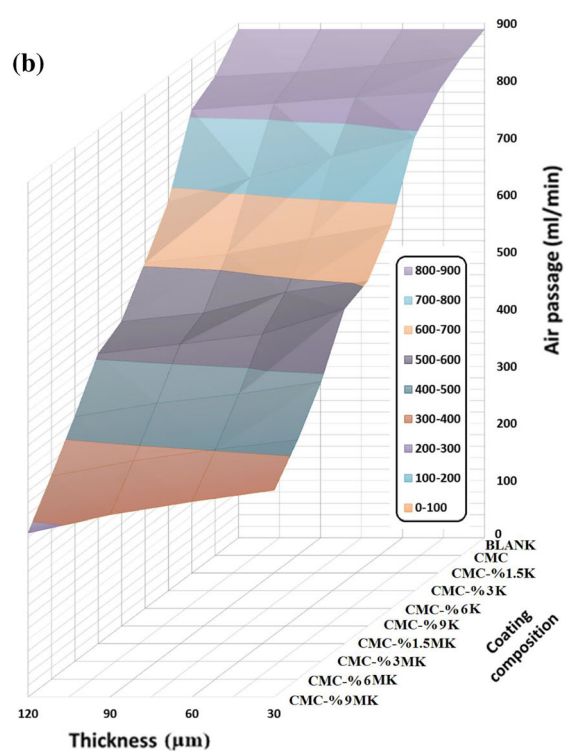
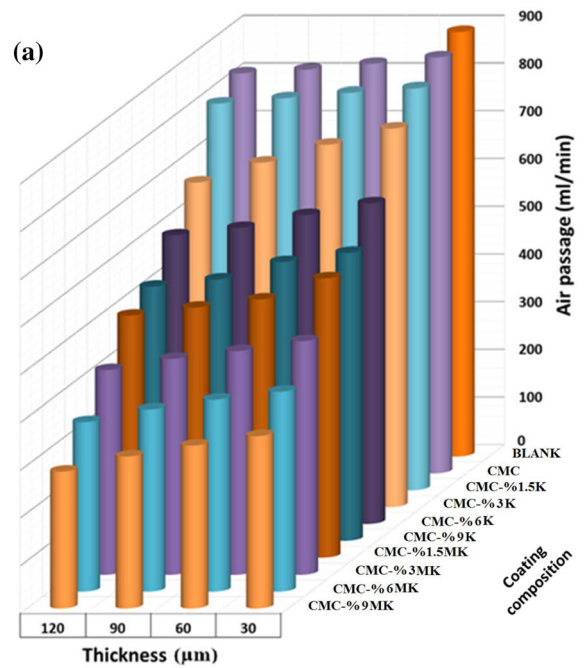


Fig. 5 Three-dimensional (3D) representation of air passage resistance variations versus coating composition and thickness ($\alpha < 0.05$); (a) air passage resistance, and (b) levels of air passage resistance changes in various coating formulations

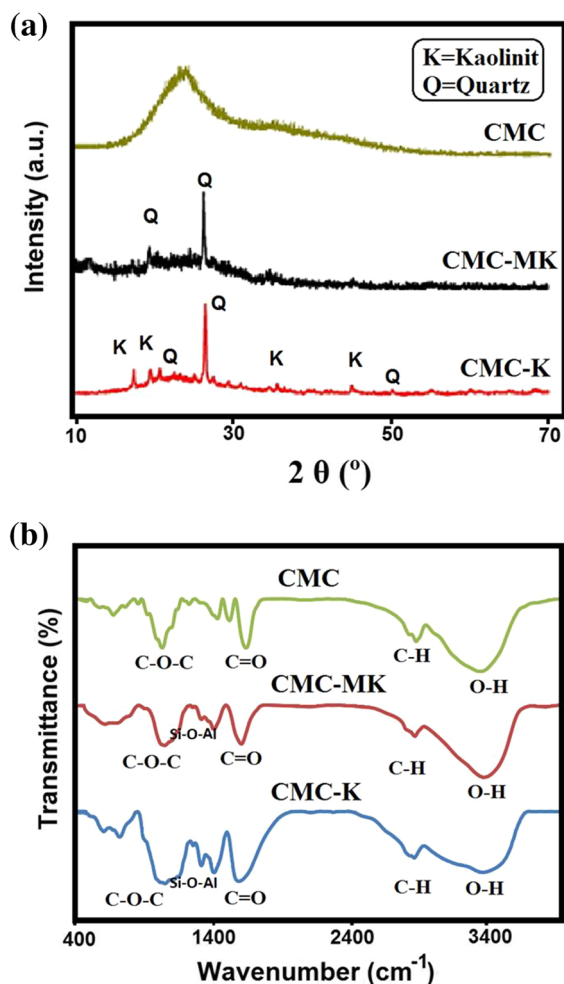


Fig. 6 (a) XRD patterns and (b) FTIR spectra of CMC, CMC-K, and CMC-MKD samples

attributed to the C–H of CH₂ and CH₃ functional groups. The presence of an absorption peak at 1600 cm^{-1} confirms the presence of carboxyl groups. The absorption bands at 1300 and 1400 cm^{-1} are related to the vibration of methyl group and the flexural vibration of hydroxyl group, respectively. The absorption bands appeared at 1050 and 1230 cm^{-1} are attributed to the symmetrical of C–O–C and CH₂–O–CH₂ groups, respectively. The bond of carboxyl acid group can be observed at 1720 cm^{-1} . This vibration in CMC samples is larger than that in CMC-MK samples. However, the peaks related to the asymmetric s of carboxyl groups have shifted to larger wavenumbers. The reason for this can be attributed to the strong interaction with metal ions. Comparing the FTIR

spectra, two samples of CMC-K and CMC-MK, peaks in the area at 400–800 cm^{-1} have appeared. They can be attributed to metakaolin and kaolin sheets' vibration bonds due to T–O and Si–O–T (T = Si, Al) bonds. The peak at 3440 cm^{-1} in both CMC-K and CMC-MK samples belong to the vibrations of hydroxyl group (O–H). The peak observed in the range of 2850–2920 cm^{-1} is related to the C–H stretching vibration, which is present in both nanocomposites (CMC-K and CMC-MK), this agent exists in different forms (–CH₂, –CH, –CH₃). The band at 1650 cm^{-1} is related to the COO. This functional group (carboxylate) which exists in both nanocomposites. Other vibrational bands typical of CMC carboxylate groups appear in the fingerprint region.

In the FTIR spectra of CMC-K and CMC-MK samples in Fig. 6b, the absorption peak in the range of 400–800 cm^{-1} is related to T–O and Si–O–T (T = Si, Al) vibration in kaolin and metakaolin. The kaolin characteristic peak at 642 cm^{-1} wavenumber, attributed to the Si–O–Al bonds, disappeared in metakaolin. This indicates the increased activity and reactivity of metakaolin relative to kaolin. The peak at 912 cm^{-1} in the kaolin spectrum is also due to the Al–OH bonds with the six-coordinate. This peak disappeared in the metakaolin spectrum. Hexagonal units of Al are converted to tetragonal (Mgbemena et al. 2013; Gaikwad et al. 2015; Demirc et al. 2020). The tetragonal bending vibrations of Si–O–Al appeared at 648 cm^{-1} , confirming the presence of metakaolin nanoparticles. The results showed no significant change in the structure of CMC after the addition of MK nanoparticles. In addition, the of Si–O–Al bond can be seen at 650 cm^{-1} which has shifted to lower frequencies; the of C = O bond of CMC has also shifted to lower frequencies in the CMC-MK sample. The FTIR and XRD results are consistent with those reported by Alfred D. French (2020).

The surface morphology of papers coated with different thicknesses of CMC-K (Fig. 7a) and CMC-MK (Fig. 7b) were evaluated by means of SEM. As shown in Fig. 7a1–a3, the coating formulation contains nanokaolin that could fill the pores to a certain extent, but they could not form a complete layer on the surface of the paper. In Fig. 7b2, the beginning of the formation of a complete layer is observed. A complete layer on paper can be seen in Fig. 7b3 for CMC-9%MK-120 sample, but accumulation and clustering

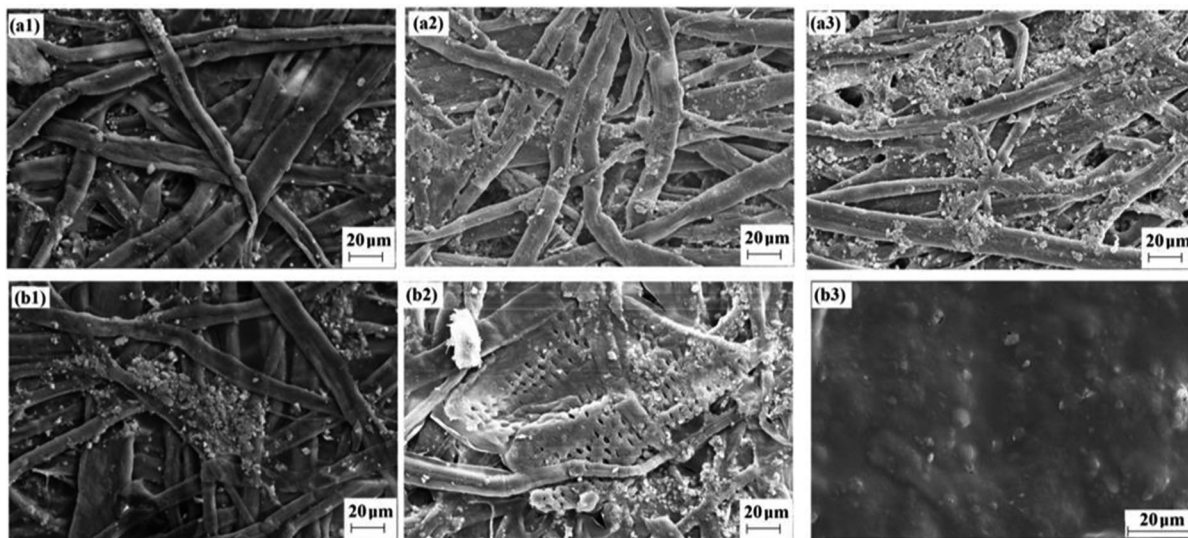


Fig. 7 SEM images of coating on paper with different thicknesses: (a1) CMC-9% K-60, (a2) CMC-9% K-90, (a3) CMC-9% K-120, (b1) CMC-9% MK-60, (b2) CMC-9% MK-90, and (b3) CMC-9% MK-120

occurred in other samples. SEM images show that the nanoparticles have filled the paper pores, which is in good accordance with the air permeability resistance and mechanical tests results. CMC-MK samples showed the lowest air passage, indicating a limited space between the pores. According to the SEM images, CMC-9%MK-120 sample showed better dispersion and created a more uniform layer on the paper. In contrast, CMC-9%K-120 was not able to form a uniform layer on the paper.

Conclusion

The current study reports the successful synthesis of kaolin and metakaolin from paper waste by heat treatment and acid washing with hydrochloric acid (HCl). The nanoparticles synthesized via planetary ball milling were confirmed by XRD, FTIR, and SEM analyses. XRD patterns showed strong and sharp diffraction peaks corresponding to the well crystalline triclinic crystal structure. No additional peak was observed in XRD, indicating the high purity of the extracted kaolin from paper waste. Conversion of kaolin to metakaolin was also confirmed by XRD and FTIR analyses. Planetary ball mill was used to produce nanokaolin and nanometakaolin particles. According to the SEM images confirmed that the particles are

spherical with sizes less than 100 nm. The permeability and mechanical properties of making handmade papers coated with CMC, CMC-kaolin, and CMC-metakaolin were also investigated. The highest tensile index, burst index, air permeability resistance, and strain ($80.78 \frac{N.m}{g}$, $5.24 \frac{kPa.m^2}{g}$, $286.66 \frac{ml}{min}$, and 3.09%, respectively) were obtained for CMC-9%MK-120 sample. Also, microstructural studies confirmed that CMC-9% MK-120 is the only sample that can fill the pores and create a complete layer on the surface of paper. Thus, CMC-9% MK-120 can be considered as the optimum sample with the best dispersion and layer formation ability. The results confirmed the significant effect of the synthesized nanomaterials on the permeability and mechanical properties of the coated papers. Therefore, such environment-friendly nano-biocomposite has the potential to be used in the packaging industry, especially where high mechanical properties are required.

Funding This investigation was supported by Sari Agricultural Sciences and Natural Resources University, and Department of Nano Materials and Nano Coatings, Institute for Color Science and Technology.

Declarations

Conflict of interest The authors declare no conflict of interest.

Ethical approval This article does not contain any studies with human participants or animals performed by any authors.

References

- Asadi M, Naghizadeh R, Nemati A, Arzaniaan K, Nassiri R (2012) Synthesis and microstructural properties of a geopolymer cement with high silica materials. *J Ceram Process Res* 13(4):425–428
- Asadi M, Nemati A, Naghizadeh R, Arzani K, Fahim J (2013) Effect of temperature and activator molar of Na₂O to SiO₂ in the process of synthesis and microstructure of cement geopolymer. *Adv Mater Process* 3(1):3–10
- Demirci S, Sutekin D, Sahiner N (2020) Polymeric composites based on carboxymethyl cellulose cryogel and conductive polymers: synthesis and characterization. *J Compos Sci* 4(2):33–41
- French Alfred D (2020) Increment in evolution of cellulose crystallinity analysis. *Cellulose* 27:5445–5448
- Gaikwad K, Seonghyuk O (2015) Overview on in polymer-nano clay composite paper coating for packaging application. *J Material Sci Eng* 4(1):151
- Gurram RN, Shannag MA, Lecher NJ, Duncan SM, Singasaas EL, Alkasrawi M (2015) Bioconversion of paper mill sludge to bioethanol in the presence of accelerants or hydrogen peroxide pretreatment. *Bioresour Technol* 192:529–532
- Hubbe M, Gill RA (2016) Fillers for papermaking: a review of their properties, usage practices, and their mechanistic role. *BioRes* 11(1):2886–2963
- Huseien G, Mirza J, Ismail M, Ghoshal SK, MohdAriffin MA (2018) Effect of metakaolin replaced granulated blast furnace slag on fresh and early strength properties of geopolymer mortar. *Ain Shams Eng J* 9(4):1557–1566
- Kenne Diffo BB, Elimbi A, Cyr M, Manga JD (2015) Effect of the rate of calcination of kaolin on the properties of metakaolin-based geopolymers. *J Asian Ceram Soc* 3(1):130–138
- Li X, Rao F, Song S, Mario A, Corona-Arroyo LNO, Aguilar-Reyes, (2018) Effects of aggregates on the mechanical properties and microstructure of geothermal metakaolin-based geopolymers. *Results Phys* 11:267–273
- Lorentz B, Shanahan N, Stetsko YP, Zayed A (2018) Characterization of Florida kaolin clays using multiple-technique approach. *Appl Clay Sci* 161:326–333
- Menzel C, Koch K (2014) Impact of the coating process on the molecular structure of starch-based barrier coatings. *J Appl Polym Sci* 131(23):4119–41190
- Mgbemena CO, Ibekwe NO, Sukumar R, Menon A (2013) Characterization of Kaolin intercalates of oleochemicals derived from rubber seed (*Hevea brasiliensis*) and tea seed (*Camelia sinensis*) oils. *J King Saud Univ Sci* 25:149–155
- Murray HH (1961) Industrial applications of kaolin. *Clays Clay Miner* 10:291–298
- Morsy FA, El-Sherbiny S, Hassan MS, Heba FM (2014) Modification and evaluation of Egyptian kaolinite as pigment for paper coating. *Powder Technol* 264:430–438
- Prasetyo J, Park EY (2013) Waste paper sludge as a potential biomass for bio-ethanol production. *Korean J Chem Eng* 30(2):253–261
- Rakhimova NR, Rakhimova NR (2019) Reaction products, structure and properties of alkali-activated metakaolin cements incorporated with supplementary materials – a review. *J Mater Res Technol* 8(1):1522–1531
- Rastogi V, Samyn P (2015) Bio-based coatings for paper applications. *Coatings* 5(4):887–930
- Rong M, Zhang M, Ruan WH (2006) Surface modification of nanoscale fillers for improving properties of polymer nanocomposites: a review. *J Mater Sci Technol* 22:787–796
- Singhal AK, Kumar S, Gupta S, Bhardwaj S, Avantha R (2015) Calcium sulphate as pigment for improved functional properties of coated paper. *PROG ORG COAT* 79:31–36
- Walkley B, Hussein O, Ke X, Bernal S (2019) Incorporation of strontium and calcium in geopolymer gels. *J Hazard Mater* 382:121015

Publisher's Note Springer Nature remains neutral with regard to jurisdictional claims in published maps and institutional affiliations.